Combining structural rugosity and crystal packing comparison: A route to more polymorphs?

Riccardo Montis[a,b]*, Michael B Hursthouse[b], John Kendrick[c], Jason Howe[b] and Richard J. Whitby[b].

[a] Università degli Studi di Urbino "Carlo Bo", Via Aurelio Saffi, 2 – 61029 Urbino PU – Italy

[b]University of Southampton, University Road, Southampton, SO17 1BJ, UK

[c]University of Leeds, Leeds, LS2 9JT, UK

Abstract

In this study we have combined structural comparisons and the rugosity model to investigate experimental and predicted crystal structures from previous results of a CSP study on a group of three rigid, planar small molecules, 2-methyl-, 3-methyl- and 2,3-dimethyl-benzo[b]thiophene 1,1-dioxide. The results of the crystal structure comparisons provided some insights on the possibility that pairs of predictions, close in energy, might be related by potential phase transitions. In particular, we observed that for some pairs of predictions, a transformation from one type of crystal packing to the other would only require small shifts between adjacent molecules. This raised the question whether only few of these predictions can effectively be experimentally isolated. The calculations of the structural rugosity, a parameter that correlates surface rugosity with ease of crystallization, indicated smooth surfaces only for few predictions. With the aim to isolate new polymorphs, we performed a small experimental study, limited to few common solvents and crystallizations from the melt. Crystallizations from the melt selectively produced single-crystals of new polymorphs for the 3-methyl – and the 2,3-methyl- benzothiophene derivatives. These showed good correlations with the above calculations, suggesting that the combination of crystal structure analysis and experimental screening might represent a useful approach in polymorphism screenings.

Introduction

Why don't we find more polymorphs?[1] This simple question perfectly summarises the complexity related to experimental and computational aspects of polymorphism screenings. In fact, despite the major advancements in this fascinating research topic, polymorphism still represents a challenging aspect of structural crystallography and crystal engineering.[2,3]

The term polymorphism describes the possibility for a given molecule to adopt more than one crystal structure, resulting in distinct crystal forms with different chemical and physical

properties.[4,5] Especially for molecules with industrial and commercial applications, differences in these properties are critical and might affect the quality and the performance of the final product, resulting in potential issues in its development, commercialization and storage. [6–8]

Accordingly, experimental and computational methods have been extensively applied to polymorphism screening, especially in the pharmaceutical field.[9,10] The aim is to predict and identify any relevant polymorphic form for a given pharmaceutical compound and, consequently, define the experimental conditions to obtain them. In practice, polymorphism is a phenomenon influenced by several variables and defining a general protocol is still challenging for several reasons.[3]

While some compounds[11] seem to be more prone to crystallize in different polymorphic forms, others[2] still remain monomorphic. Additionally, some of them are easier to crystallise [12] while others, in order to be isolated, require specific and, sometimes, complex experimental conditions. [13] Crystallizations from the melt[14], at high pressure[15] or in the presence of specific additives or impurities[16–18] able to promote or prevent the observation of specific polymorphic forms, might represent a selective route to polymorphic forms otherwise difficult to isolate.

Crystal structure prediction (CSP) methods have, over the last twenty years, progressed significantly,[19,20] becoming an important tool in polymorphism screening. For a given molecule, CSP often provide quite large sets of thermodynamically feasible structures, defining what is termed the "Crystal Energy Landscape". However, CSP invariably predicts far more potential polymorphs than are experimentally found, even when extensive experimental screenings are made. Reasons for this discrepancy can be various and some of them have been previously discussed.[1,3,13]

Polymorphism is the result of a subtle balance between thermodynamic and kinetics factors. Some polymorphs nucleate or crystallize more rapidly[3,9] than others; some of them can undergo spontaneous phase transitions to a more stable form.[13] Unfortunately, these factors are not taken into consideration by crystal energy landscapes.

Crystal structure analysis, when combined with complementary characterization techniques, may represent a further useful tool for polymorph screening.[21–25] This approach can be applied not only to experimental polymorphs, but also to families of predicted structures.

Based upon the theme of the above discussion, we have been exploring the idea that detailed crystal structure comparisons of predicted and experimental polymorphs, of the kind we have been using to analyse the structures of derivative families of compounds,[21,26–29] may represent a further useful tool for polymorph screening. Indeed, the identification in a group of predicted structures of common and robust supramolecular arrangements, also observed in experimental

structures of the same compound, might help in discriminating which structure, within the crystal energy landscape, would seem likely to be experimentally isolated.[13] Furthermore, the identification of high structural similarities in clusters of predicted forms close in energy, might help in identifying pairs or groups of structures which may transform one into the other, during the nucleation/crystal growth stages, or by spontaneous solid-solid phase transitions, thus preventing the observation of some metastable forms. This approach has been previously applied to identify potential mechanisms for single crystal to single crystal phase transitions.[30] The recent development of automated software for structural comparison[31,32] allows a fast and accurate identification of structural similarities even in large families of related crystal structures.

Another useful tool based on structural features is the structural rugosity.[12] This concept, recently proposed by Cruz-Cabeza and co-workers, is based on the molecular rugosity model by Bryant, Maloney and Sykes[33] and correlates kinetic pathways and crystal structure features. The basic idea is that polymorphs with smooth structural surfaces have lower interfacial tensions[34] and consequently nucleate and grow faster[35] than polymorphs with rough surfaces and a higher interfacial tension.

In this present paper we aim to combine these two tools to investigate a family of predicted polymorphs and identify which might be amenable to experimental discovery. For this study, we have used the results of a CSP calculation previously published by Asmadi et al.[36] on a group of three rigid, planar small molecules (see Scheme 1), 2-methyl-, 3-methyl- and 2,3-dimethyl-benzo[b]thiophene 1,1-dioxide (from now on referred to as 2-Me, 3-Me and 23-Me). Firstly, we carried out a crystal packing comparison of the first ten most stable predicted structures of each of the three energy landscapes, using the XPac program.[31] The comparison was also extended to predictions belonging to different landscapes to identify whether the different position of substitution in the three methyl- benzothiophene derivatives can promote specific supramolecular arrangements in the solid state.

For each structure of the energy landscape, we then calculated the structural rugosity to see whether any of the predictions can represents a potential target for experimental screenings.

Finally, considering that only one experimental form of each molecule was known,[37,38] we decided to see if any new polymorph could be experimentally isolated.

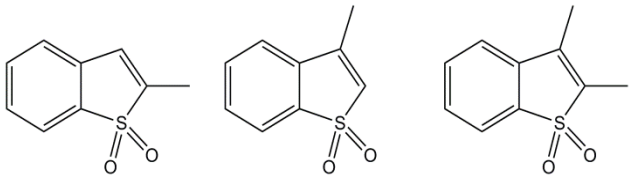

Scheme 1 2-methyl-, 3-methyl- and 2,3-dimethyl-benzothiophene-1,1-dioxides (2-Me, 3-Me and 2,3-Me).

Experimental

Synthesis of 2-Me, 3-Me and 23-Me.

2-Methylbenzo[b]thiophene was prepared from benzo[b]thiophene via lithiation and alkylation with methyl iodide.[39] 3-Methylbenzo[b]thiophene was prepared from 3-bromobenzo[b]thiophene[40] via bromine / lithium exchange followed by methylation with methyl iodide. 2,3-Dimethylbenzo[b]thiopene was prepared from diphenylzirconocene and 2-butyne using the method reported by Buchwald.[41] The benzothiophenes were oxidised to the corresponding sulfones using hydrogen peroxide in acetic acid.

Details of the synthesis, purification and characterization of each methyl derivative are described in Supplementary Information (Section S1).

Fourier Transform Infrared (FT-IR) Spectroscopy

Fourier Transform Infrared (FT-IR) spectra were recorded with a Nicolet FT-IR Golden Gate Spectrometer (4000-400 cm^{-1}) at an instrument resolution of 4 cm^{-1} (32 scans per spectrum).

Thermal Analysis

Differential Scanning Calorimetry (DSC) measurements were performed on a Mettler Toledo DSC821e low temperature differential scanning calorimeter fitted with a 34 place autosampler controlled by Star^e Software. The measurements were carried out under spectroscopic grade nitrogen as a protective and purge gas at atmospheric pressure in standard 40 μL aluminium crucibles. The instrument was calibrated for temperature accuracy using an indium standard. Approximately 1-5 mg samples were encapsulated in 40 μL Al-Pans which were hermetically sealed and heated at three different heating rates (2, 10 and 90 °C / min).

Thermomicroscopy investigations were carried out on a Leica DM2500M optical polarizing microscope equipped with hot stage apparatus controlled by a Mettler Toledo FP90 central processor. Samples were heated over the temperature range of 25–200 °C at a constant heating-

cooling rate of 10 °C /min. Microphotographs were recorded with a CCD camera attached to the Leica DM2500M microscope at 2 s time intervals using Studio Capture software.

Crystallizations

The three synthesised compounds were crystallised from methanol (MeOH), ethanol (EtOH), n-propanol (PropOH), ethyl acetate (AcOEt), dichloromethane (DCM) and mixtures of acetonitrile/water (MeCN/H_2O 1:1) and methanol/water (MeOH/H_2O 1:1). Approximately 20-30 mg of substance was dissolved into the solvent and left to evaporate at room temperature (see Supporting Information Table S2).

Crystallization from the melt was also carried out, using a Leica DM2500M optical polarizing microscope equipped with hot stage apparatus controlled by a Mettler Toledo FP90 central processor. Approximately 2-5 mg of substance were placed on the glass slide with a glass cover sealed with grease. The sample was then heated until a melting process started and then cooled down slowly to grow crystals. The heating-cooling process was repeated several times to melt most of crystals and isolate suitable seeds. At this stage, the cover slide was quickly removed, the crystal covered with silicon oil and excised with a scalpel.

X-Ray Diffraction Studies

Single crystal diffraction data were recorded on a Nonius KappaCCD diffractometer situated at the window of a Bruker Nonius FR591 rotating anode generator equipped with a molybdenum target (λ Mo-kα = 0.71073Å) and driven by COLLECT,[42] and DENZO[43] software. Structures were determined using the direct methods procedure in SHELXS 97[44] and refined by full-matrix least squares on F^2 using SHELXL97,[44,45] (within the Olex2[46]).

Data were corrected for absorption effects by means of comparison of equivalent reflections using the program SADABS.[47] Non-hydrogen atoms were refined anisotropically, hydrogen atoms, were fixed in idealised positions with their displacement parameters riding on the values of their parent atoms (1.2 *Ueq*). Single-crystal X-ray diffraction data are reported in Table S3.

XPac analysis

The search for crystal structure similarities was made using the XPac software,[31] the use of which is fully described in earlier papers.[31,48] Calculations were made for the six pairwise combinations of the molecular sets – (2-Me / 2-Me, 3-Me / 3-Me, 23-Me / 23- Me, 2-Me / 3-Me, 2-Me / 23-Me and 3-Me / 23-Me) by selecting the most representative

Corresponding_Ordered_Sets of_Points (COSPs) for the relevant molecular pairs. These consist of fragments of connected atoms in common between the set of molecules under comparison. The software compares the relative orientations and positioning of the COSPs of the sets of structures, identifying any similar molecular arrangements. These can have 0-D (eg. dimers or generally small clusters of molecules), 1-D (eg. infinite chains, tapes, rods or stacks of molecules), 2-D (sheets or slabs) and 3-D (isostructural or isomorphic) arrangements. For each similarity found, a dissimilarity index is also provided, and this parameter represents the deviation from perfect geometrical similarity, and so we look for values lower than a pre-set limit, which we take to confirm a similarity. Details of the COSPs selected for the analysis and the resulting dissimilarity indexes, corresponding lattice vectors and symmetry codes for 1-D, 2-D and 3-D similarities, are reported in Supporting Information (Tables S4-S9).

Structural Rugosity

Structural rugosity calculations have been carried out using a script developed by the Cruz-Cabeza's group, using the CSD Python API.[12] This method is based on the molecular rugosity model by Bryant, Maloney and Sykes,[33] that calculates the degree of interpenetration between adjacent (hkl) faces ($R^{(hkl)}_{depth}$) as the distance between the highest atom in a given (hkl) crystal slice and the average plane between that slice and the adjacent slice. A negative value of the rugosity parameter indicates interpenetrated layers while positive values indicate a separation between adjacent layers and, consequently, no interpenetration.

The Python script developed by the Cruz-Cabeza's group calculates the overall normalized rugosity ($\bar{R}^N_{depth}$) as the sum of the rugosities of each hkl face and normalizing them by their face d-spacing ($d^{(hkl)}$ in Å) and weighting them by the BFDH morphological importance of each of the (hkl) faces ($w^{\{hkl\}}$), as reported in the equation below.[12]

$$\bar{R}^N_{depth} = \sum_{\{hkl\}} w^{\{hkl\}} R^{(hkl)}_{depth} / d^{(hkl)}$$

Polymorphs or, in general, structures with rough (negative $\bar{R}^N_{depth}$) surfaces are difficult to crystallize while polymorphs with smoother surfaces (less negative $\bar{R}^N_{depth}$ or with $\bar{R}^N_{depth} > 0$) are easier to crystallize.

Results and Discussion.

Structural Comparison.

As reported in the previous study by Asmadi et al,[36] the known experimental structures of 2-Me (GAKPEN),[37] 3-Me (GAKPIR)[37] and 23-Me (GAPMAL) [38] corresponded to the first, second and third most stable structures in the respective prediction lists.

We summarise these results in Table 1, where the ten lowest energy predictions optimised with the hybrid method are reported. The fact that the experimental structures for 3-Me and 23-Me had energies slightly above the respective global minima posed the question as to whether these differences in energy just reflect variations inherent to the calculations or that the predicted lower energy structures could be potential new polymorphs.[36]

Table 1. Summary of the ten lowest energy predictions optimised with the hybrid method. The experimental structures for 2-Me (CSD code GAKPEN), 3-Me (CSD code GAKPIR) and 23-Me (CSD code GAPMAL) are indicated by shading.

2-Me				3-Me				23-Me			
Rank	**ΔE [kJmol^{-1}]**	**density [g cm^{-3}]**	**S.G.**	**Rank**	**ΔE [kJmol^{-1}]**	**density [g cm^{-3}]**	**S.G.**	**Rank**	**ΔE [kJmol^{-1}]**	**density [g cm^{-3}]**	**S.G.**
01	0.0000	1.440	$P2_1/c$	**01**	0.0000	1.441	$P2_1/c$	**01**	0.0000	1.385	*Pbca*
02	0.4018	1.431	*Pbca*	**02**	0.3935	1.410	$P2_12_12_1$	**02**	0.0402	1.378	$P2_1/c$
03	1.0716	1.443	$P2_1/c$	**03**	0.4856	1.436	*Pbcn*	**03**	0.1206	1.393	*P-1*
04	1.3897	1.433	$P2_1/c$	**04**	0.6697	1.443	$P2_1/c$	**04**	0.7334	1.382	$P2_1/c$
05	1.5320	1.420	$P2_1/c$	**05**	1.2306	1.425	$P2_1/c$	**05**	0.7936	1.390	$P2_1/c$
06	2.3692	1.433	$P2_1/c$	**06**	1.2641	1.431	$P2_1/c$	**06**	1.2658	1.381	$P2_12_12_1$
07	2.6957	1.388	$P2_1/c$	**07**	1.9841	1.410	$P2_1/c$	**07**	1.2658	1.373	$P2_1/c$
08	3.2231	1.397	$P2_1$	**08**	2.3022	1.406	$P2_1/c$	**08**	1.4768	1.387	$P2_1/c$
09	3.6249	1.420	$P2_1/c$	**09**	2.6203	1.419	*Pbca*	**09**	1.6073	1.376	$P2_1/c$
10	3.6835	1.414	*P-1*	**10**	2.7208	1.420	$P2_1/c$	**10**	2.0494	1.388	$P2_1/c$

Firstly, we used the XPac software[31] to compare the predicted structures (comparison 2-Me_01-10 /2- Me_01-10, 3-Me_01-10 /3-Me_01-10 and 23-Me_01-10 / 23-Me_01-10) with the aim to identify any potential robust and recurring molecular arrangement within each set of predictions. We then extended the comparison to predictions belonging to different sets (comparisons 2- Me_01-10 / 3- Me_01-10, 2-Me_01-10 / 23-Me_01-10 and 3-Me_01-10 / 23-Me_01-10), to identify whether the different position of substitution promotes differences in the crystal packing. The matrix reported in Fig. 1 summarizes the results of the six comparisons. These are indicated by the use of different colours for the different similarities in Figure 1. Details and descriptions of 1-D, 2-D and 3-D similarities are reported in Supplementary Information (see Tables S4-S9). 0-D similarities, such as dimers or in general

Figure 1. Structural comparison in 2-Me 01-10, 3- Me 01-10 and 23-Me 01-10. 1-D, 2-D and 3-D similarities are indicated in light-blue, yellow and red.

oligomeric molecular arrangements, have been omitted from the analysis since not relevant for the discussion.

Of particular interest is the different distribution of the structural similarities within the six comparisons. Table 2 shows the number of different structural similarities for each comparison.

Table 2. Distribution of the structural similarities for the crystal structure comparison.

Comparisons	1-D	2-D	3-D	total
2-Me_01-10 / 2-Me_01-10	3	3	0	6
3-Me_01-10 / 3-Me_01-10	11	1	0	12
23-Me_01-10 / 23-Me_01-10	19	7	0	26
2-Me_01-10 / 3-Me_01-10	17	2	0	19
2-Me_01-10 / 23-Me_01-10	28	7	2	37
3-Me_01-10 / 23-Me_01-10	32	3	0	35

Table 2 lists the distribution of 1-D, 2-D and 3-D similarities for each set of comparison.

In general, calculation involving the family of predictions of the 23-Me derivative show a larger number of similarities. This is particularly evident in the case of comparisons 2-Me_01-10/23-Me_01-10 and 3-Me_01-10 / 23-Me_01-10, where the high number of structural similarities most likely reflect the fact that 23-Me has common molecular shapes with both 2-Me and 3-Me compounds.

Interestingly, the comparison 2-Me_01-10 / 23-Me_01-10 shows the highest level of similarity, featuring two 3-D similarities, seven 2-D similarities and several 1-D similarities. This is consistent with the results of the *in-silico* seeding by Asmadi et al [36] which showed that only the 23-Me molecule could be packed in the known crystal structures of the 2-Me, resulting in a crystal structure within the list of ten most stable predictions.

We then analysed in detail the structural relationships, focusing, in particular, on the 2-D and 3-D similarities. The results are summarised in the relationship diagram in Figure 2, where we also included the most relevant 1-D similarities (see below). Apart the two 3-D similarities which relate the pairs 2-Me_01 / 23-Me_02 and 2-Me_10 / 23-Me_03, we also identified a total of nine 2-D similarities (A-I) involving all the predictions. These are also represented in Figure 3. In particular, similarities A-B relate pairs of structures within the family of predictions of 2-Me (2-Me_05/2-Me_08, 2-Me_04/2-Me_09 respectively), similarity F relates the pair 3-Me_02/3-Me_04, while the remaining similarities (C, D, E, G, H and I) are distributed within the three families.

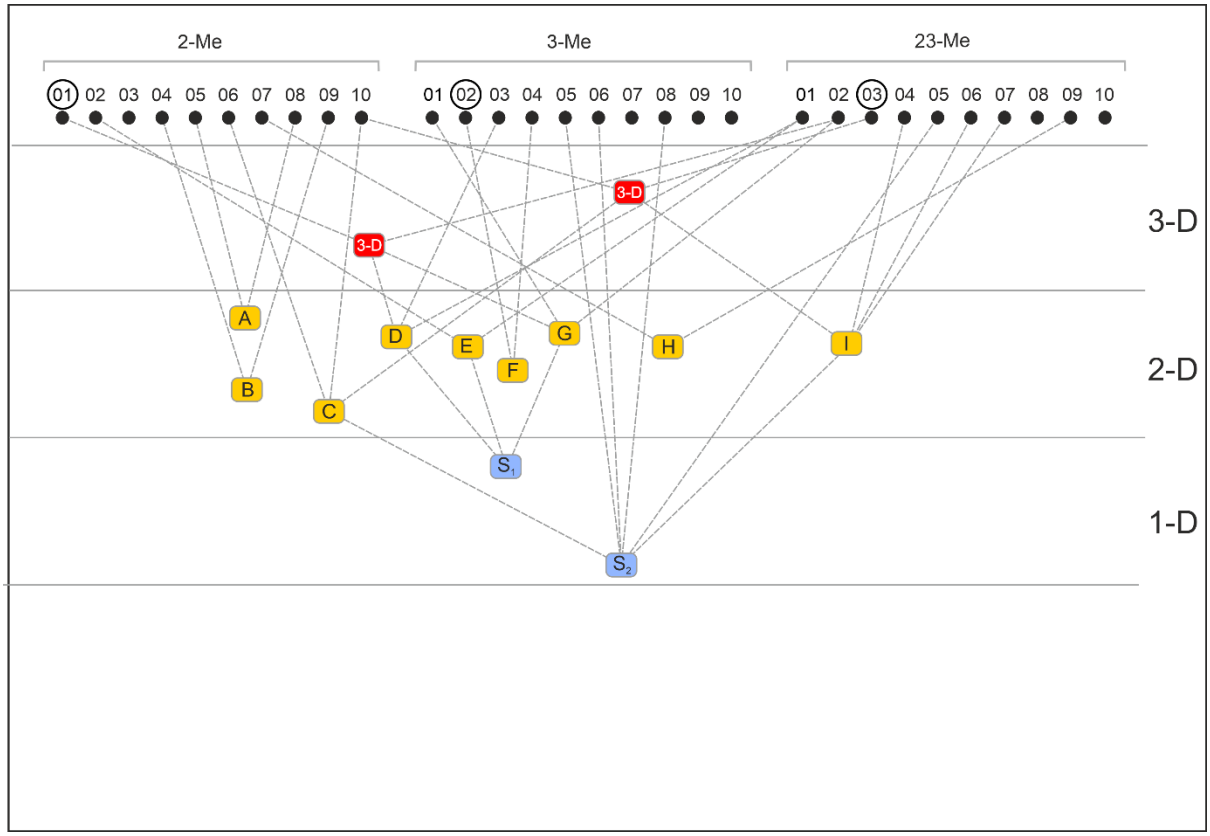

Figure.2. Structural relationships diagram for the three set of predicted structures for 2-Me (left), 3-Me (centre) and for 23-Me (right). 3-D similarities are indicated as red, 2-D similarities as yellow. Crystal structure predictions are placed on the top and, within each set, reported in order of stability from left to right. Experimental structures are indicated by a circle (1,2 and 3 respectively). Dashed connecting lines are used to indicate which structure is involved for a given similarity.

Most of the predictions are related by the five similarities C, D, E, F and G. Similarities D, E and G, relate the lowest energy structures of each set of predictions (2-Me_01, 2-Me_02, 3-Me_01, 23-Me_01 and 23-Me_02). Interestingly, the majority of the similarities contain the two 1-D stacking arrangements S1 and S2 (see Figure 2 and 3). S1 is part of the 2-D similarities D, E and G and consists of a 1-D face-to-face stack of molecules (Figure 3 b) connected to each other by π…π contacts that, in the case of the 3-Me and 23-Me structures, are supported by C-H…O interactions, involving methyl groups. This is differently assembled in similarities D and E and G, forming a zig-zag arrangement in the case of D and E a linear arrangement in the case of G (Figure 3 a).

The stacking arrangement S2 (Figure 3) is only observed as part of the similarities C and I, that mostly involve structures belonging to the family of 23-Me predictions and few predictions of the 2-Me derivative. The stacking arrangement S2 differs to S1 for the different orientation of the molecules along the direction of stacking (Figure 3).

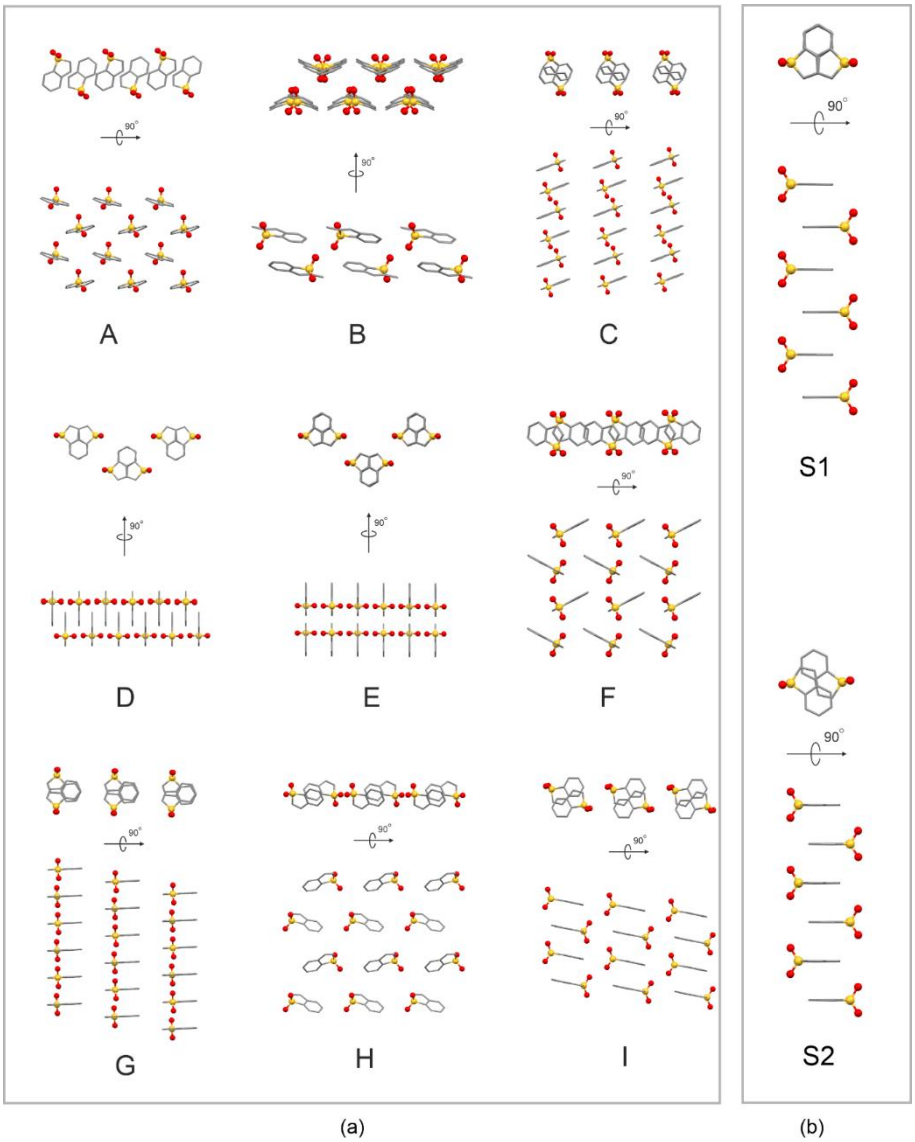

Figure 3. 2-D similarities A-I. Hydrogens and methyl groups have been removed for clarity

Like the previous case, molecules are connected to each other via π…π, and, in the case of structures of the 23-Me derivatives, by weak C-H…O interactions involving the methyl group in position 3.

Figure 4 shows the three energy landscapes for the set of predictions. The plot also reports the distribution of the two stacking arrangements S1 and S2 within the set of predictions. Interestingly, the two types of stacking relate most of the predictions and, most importantly, stack S1 represents a common feature among most of the lowest energy predictions (see Figure 4).

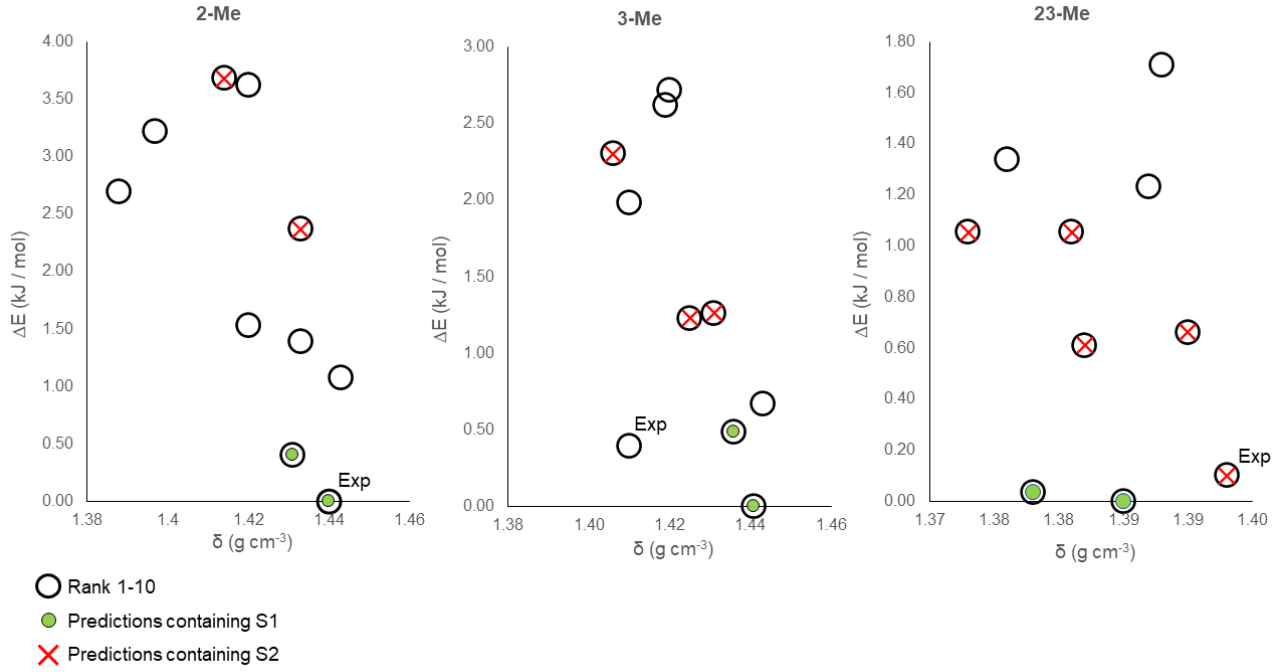

Figure 4. Energy landscape for 2-Me, 3-Me and 23-Me. Structures containing the stacking S1 and S2 are indicated by (●) and (✕) respectively. The experimental structures for 2-Me (CSD code GAKPEN), 3-Me (CSD code GAKPIR) and 23-Me (CSD code GAPMAL) are labelled as "Exp".

The analysis of crystal packing similarities can provide some insight on the possibility that two polymorphs can be related by a potential phase transition. However, it is important to note that this is only a qualitative approach. In fact, unless experimental evidences suggest a phase transition, the identification of a possible route of transformation between two or more polymorphs does not necessarily mean that this will occur.

The comparison of the three families of predictions for 2-Me, 3-Me and 23-Me reveals some interesting features. In general, apart the case of the pairs 2-Me06/2-Me10 and 3-Me02/3-Me04 (related by similarities C and F, see Figure S9 and S10 in Supplementary Information), for the majority of predictions related by 2-D similarities, it is possible to identify a potential route of transformation between pairs of structures (see Supplementary Information, section S4). In the case of predictions 2-Me08/2-Me05, the transformation would involve rotations and tilting of molecules (Figure S7in Supplementary Information) and perhaps this would be too complex to be plausible. In other cases, transformations between pairs of predictions only require a small relative shift between adjacent molecules (see Figures 5 and figures S8 and S11 in Supplementary Information).

This can be easily observed for the pair 2-Me_01/2-Me_02 and 23-Me_01/23-Me_02 (Figure 5 a and b), related by the similarity D, where small shift of the relative position of adjacent 2-D arrangements can ideally convert one structure into the other.

Considering the small differences in the calculated lattice energies, we believe that for each pair, most likely only one of the predicted polymorphs would be isolated experimentally. A similar consideration can be made for the predictions related by the similarity I (see Figure S11 in Supplementary Information), where, again, small shifts and energy differences open the question whether all the pairs of predicted structures can be experimentally isolated.

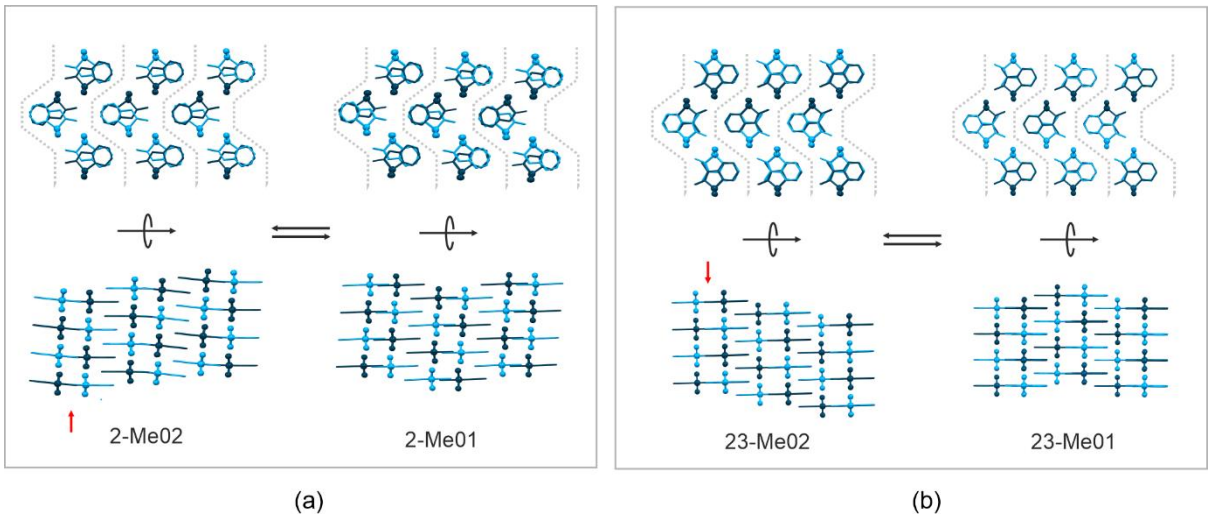

Figure 5. Crystal packing comparison for predictions showing the common similarity D. (a) 2-Me01, 2-Me02 (b) 23-Me01 and 23-Me02; The packing instances are represented along two perpendicular directions, the molecules are colour coded according to the different orientation along the stacking directions. Each instance of the similarity D is represented by grey dotted lines. Relative shifts of the 2-D arrangements along the stacking direction are indicated by vertical arrows. These identify hypothetical phase transitions between the structures compared.

Structural Rugosity.

We applied the structural rugosity model[12] to the ELSs of the three methyl derivatives 2Me, 3Me and 23Me previously published by Asmadi and co-workers.[36] The values of $\bar{R}^N_{depth}$ can range from negative values (rough polymorphs), indicating interpenetration of adjacent crystal slices, and positive values (smooth polymorphs), indicating a separation between adjacent slices. For example, a polymorph with a $\bar{R}^N_{depth}$ value of -0.2 has a larger structural rugosity than a polymorph with a $\bar{R}^N_{depth}$ value of -0.05 that, consequently, is smoother. The principle behind the model proposed by Cruz-Cabeza and co-workers (see experimental section for more details), is that polymorphs with rough surfaces have high interfacial tensions[34] and are difficult to crystallise, while polymorphs with smooth surfaces have lower interfacial tensions[34] and nucleate and grow more easily.[35] In their work, they suggested that predictions with smoothest surfaces and lying within a crystal rugosity cut-off limit of 0.20 from the smoothest polymorph,

might represent realizable forms.[12] This cut-off limit was obtained by calculating the normalized structural rugosity ($\bar{R}^N_{depth}$) on approximately 5500 polymorphs from the CSD. The results showed that about 98% of the polymorphs analyzed have a rugosity value within 0.2 units of rugosity from the smoothest polymorph.We calculated the normalized structural rugosity ($\bar{R}^N_{depth}$)[12] for the three set of predictions. The results of the calculations are shown in Figure 6, were the relative lattice energy (ΔE) of each prediction is reported versus $\bar{R}^N_{depth}$. In all the cases, the values lye within the cut-off limit of 0.2, suggesting that all these predictions can in principle be experimentally isolated.

In the case of the 2-Me derivative, the values of $\bar{R}^N_{depth}$ are all very similar. The only exception is represented by prediction 2-Me10 that is the smoothest structure. Interestingly, as discussed earlier, this prediction is isostructural with the known experimental structure for the 23-Me derivative (CSD code GAPMAL). In the case of the other two set of predictions, the $\bar{R}^N_{depth}$ is distributed over a slightly broader range of values, but still below the suggested 0.2 cut-off limit. For the 3-Me derivative, predictions 3-Me05 and 3-Me06 are the smoothest, while prediction 3-Me02, that corresponds to the experimental structure (CSD code GAKPIR), is amongst the roughest forms. Interestingly, prediction 3-Me01, shows the best combination of AE/ $\bar{R}^N_{depth}$ values, being the most stable and among the smoothest forms.

Differently to the previous cases, in the set of predictions of the 23-Me derivative, the smoothest form is represented by 23-Me03, that corresponds to the known experimental structure (CSD code GAPMAL), while the lower energy predictions 23-Me01 and 23-Me02, are amongst the roughest structures.

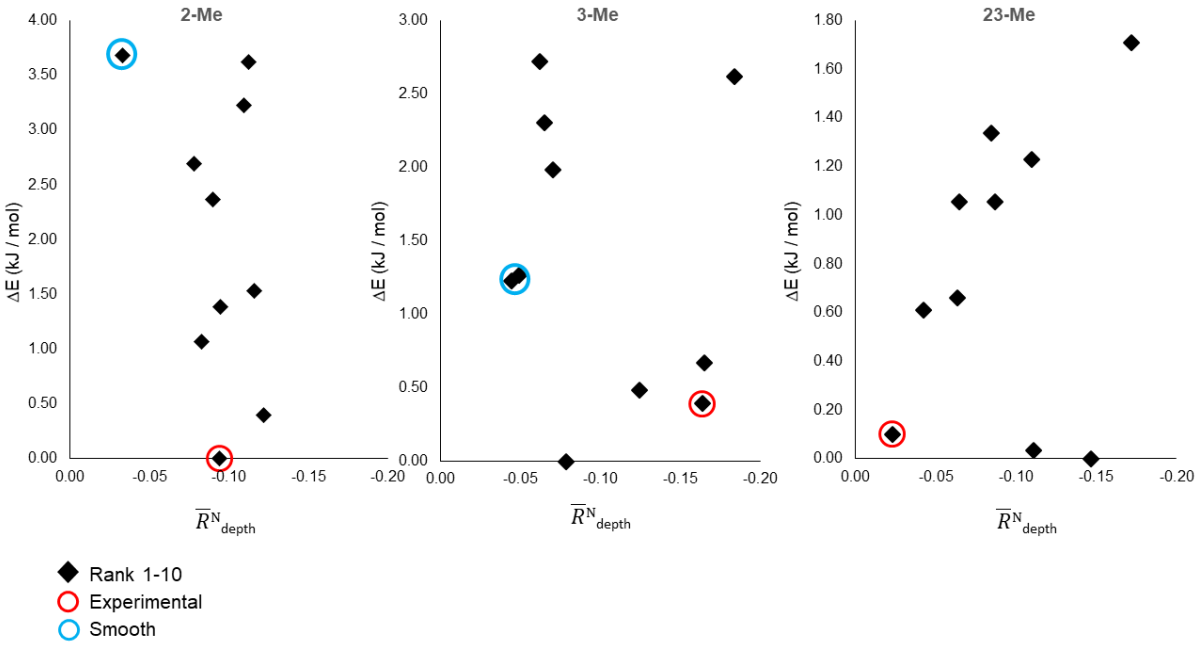

Figure 6. Relative lattice energy (ΔE) versus normalized average crystal rugosity ($\bar{R}^{N}_{depth}$) for 2-Me, 3-Me and 23-Me. The experimental structures for 2-Me (CSD code GAKPEN), 3-Me (CSD code GAKPIR) and 2, 3-Me (CSD code GAPMAL) are circled in red, while the smoothest predictions are circled in light-blue.

Experimental Study.

The three methyl derivatives of benzo[b]thiophene 1,1-dioxide 2-Me, 3-Me and 23-Me have been synthesized according to the procedures described in the experimental section (see S1 in Supplementary Information). Unfortunately, these could only be produced in small amounts (see Supplementary Information). In the case of the 2-Me compound, the product of the synthesis consisted of good quality crystals. We first determined the crystal structure by single-crystal X-ray diffraction, obtaining the same structure previously reported in the literature (CSD code GAKPEN). A similar preliminary characterization was not possible for 3-Me and 23-Me, whose products from the synthesis were in the form of a fine powder. Considering that the synthesis was not straightforward and for each derivative it required different steps, we decided to characterize the three starting materials obtained from the synthesis by differential scanning calorimetry (DSC) and Hot-Stage Microscopy (HSM), with the aim to identify any possible evidence of polymorphism for the three derivatives.

For each compound we performed a heating ramp in the temperature range 0-200 °C at 10°C/min. The three samples were then let to cool down to approximately 20°C to recrystallise and a second heating ramp at the same experimental conditions was performed. The results are showed in Figure 7 a-c.

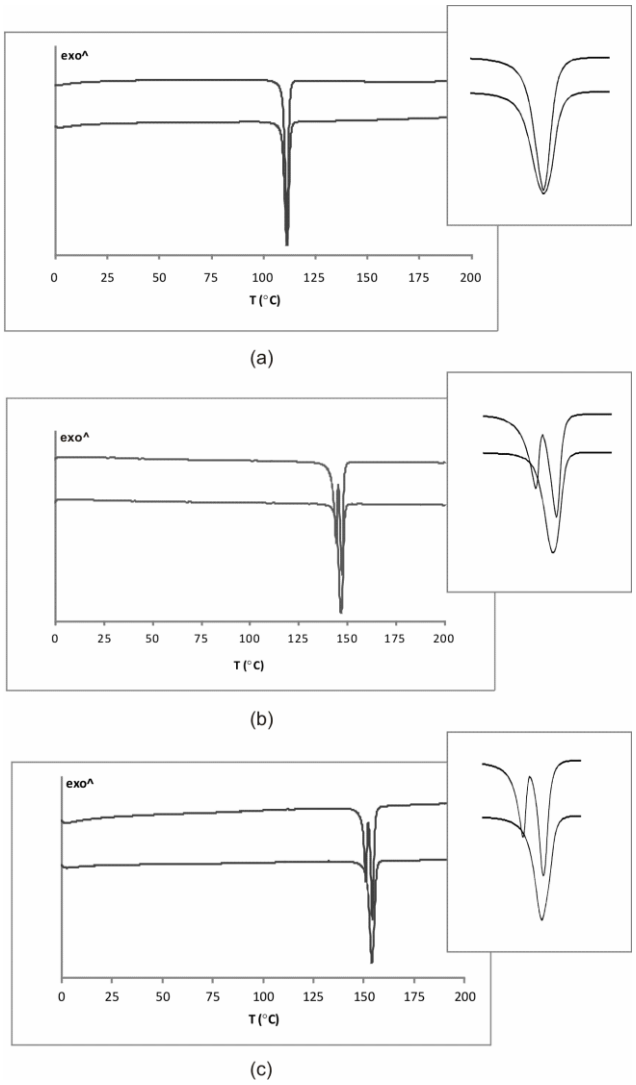

Figure 8. Differential Scanning Calorimetry (DSC) range 0-200 °C at 10°C/min. a) 2-Me; b) 3-Me; c) 23-Me. For each sample two separate measurements were made. Enlargements of the overlap regions are also shown in each case.

In the case of the 2-Me derivative, the results only showed a single endothermic peak, consistent with a melting process occurring in the range 110-111 °C (peak temperature 111.4 ± 0.6°C; onset temperature 109.7± 0.5°C). This behaviour was confirmed also by HSM, that showed a simple melting process occurring in the range 109-111 °C.

The 3-Me and the 23-Me derivatives showed some interesting results.

The 3-Me sample shows two endothermic peaks at 143.7 ± 0.3 (onset 142.1± 0.1°C) and 146.3 ± 0.4 °C (onset 145.7± 0.5°C), as reported in Figure 8 b (top curve). These, during the second heating process, become a single peak at 146.4 ± 0.3 °C (onset 145.8± 0.1°C), as shown in Figure 7 b (bottom curve).

Like in the case of 3-Me, during the first heating process 23-Me shows two endothermic peaks occurring at 149.3 ± 0.3 °C and 152.7 ± 0.2 °C respectively (onset 147.2 ± 0.3 °C and 151.2 ± 0.4 °C respectively). After recrystallization by cooling the melt (bottom curve Figure 7 c), the DSC analysis only shows a single peak at 152.8 ± 0.4 °C (onset 150.7± 0.8°C).

The HSM analysis for 3-Me and 23-Me (see Figure S2 and S3 in Supplementary Information) showed a thermal event followed by melting process consistent with those measured by DSC. However, in some cases we also observed changes in the polarization colors prior the two endothermic events, suggesting that the thermal behavior of 3-Me and 23-Me could be more complex.

The results of DSC and HSM suggested that the 3-Me and 23-Me derivatives might exist as two or more polymorphic forms. No evidence of polymorphism has been observed for the 2-Me derivative. The analysis also suggested that the higher melting forms for both, the 3-Me and 23-Me derivatives can be easily crystallized by slow cooling the melt. This method only requires a small amount of sample and often results in the isolation of metastable forms, as previously reported for the cases of nifepidine,[49] aspirin[14] and griseofulvin[50], to cite some examples.

We crystallized the three derivatives by slow evaporation, using a limited selection of solvents (see Table S2 in Supplementary Information). In all cases, these produced crystals suitable for single-crystal X-ray diffraction. The results of the determination of the unit cell parameters for these samples were consistent with the experimental known forms, [37,38] GAKPEN, GAKPIR and GAPMAL. We then analyzed these samples by DSC, obtaining the same behavior described in Figure 8, suggesting that also in the case of 3-Me and 23-Me the products from synthesis corresponded to the phases previously reported in the literature (from now labeled as 3-Me α and 23-Me α).

In order to identify the higher melting forms observed by DSC (Figure 8), we crystallized 3-Me and 23-Me from the melt, using a microscope equipped with a hot-stage. These produces good quality crystals (see Figure S4 c and d in Supplementary Information), allowing the structural determination of the higher melting forms (from now labelled as 3-Me β and 23-Me β). As expected, crystallization from the melt of the 2-Me compound uniquely produced the known form previously published by Declercq and co-workers.[37]

3-Me β.

The new polymorph 3-Me β crystallized in monoclinic crystal system (space group $P2_1/c$ **a** = 7.2483(3), **b** = 8.0417(4), **c** = 14.1246(7), β = 92.028(3), **V** = 822.79(7)). The structure shows a two-fold disorder consisting of two different orientations of the benzothiophene ring in a ratio approximately of 51-49% (Figure 8).

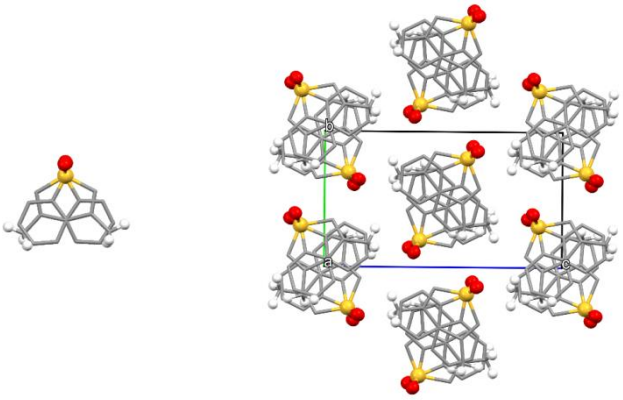

Figure 8. Disorder and crystal packing of 3-Meβ, viewed down the *a* axis of the unit cell.

The disordered molecules develop along the direction ***a*** of the unit cell, forming stacking arrangements (Figure 9 a) analogous to the arrangement S2 described above for the set of predictions. These are connected via weak C-H…O interactions (H…O distances are in the range 2.5 - 2.6 Å) to adjacent stacks along the remaining two directions of the packing (Figure 9b).

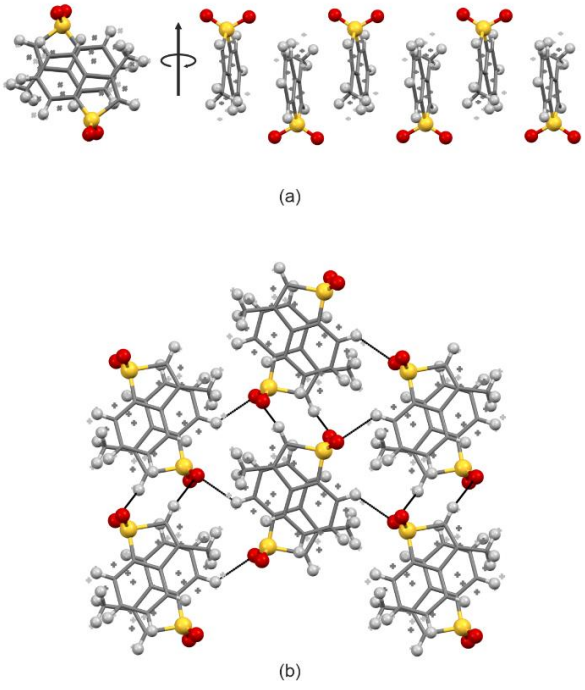

Figure 9. Crystal structure of 3-Meβ. (a)Stacking S2 for 3-Meβ, (b) crystal packing of 3-Meβ viewed down the a direction. Intermolecular interactions are indicated by black dashed lines.

23-Me β.

The new form 23-Me β crystallised in monoclinic crystal system (space group C2/c **a** = 11.3081(3), **b** = 10.9999(2), **c** = 16.1373(5), β = 106.099(2), **V** = 1928.57(9)). A representation of the crystal packing viewed down the c direction is shown in Figure 10.

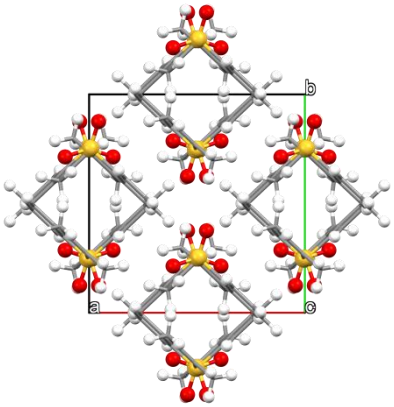

Figure 10. Crystal packing of 23-Me β, viewed down the *c* direction.

Interestingly, also in this structure we identified a stacking arrangement developing along the shortest axis which correspond to the similarity S2 (Figure 11).

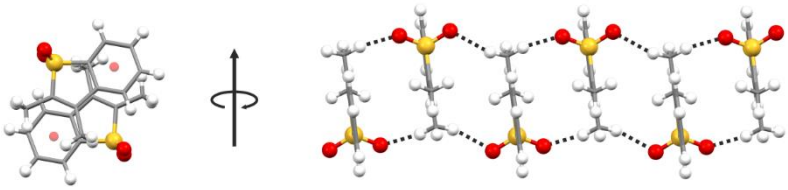

Figure 11. Stacking S2 observed in 23-Me β

In this case the adjacent molecules show a higher slippage probably due to the different shape of the molecule for presence of the second methyl group.

We compared the new polymorphs 3-Me β and 23-Me β with the set of predictions previously published. For the case of 3-Me, in order to apply the XPac procedure, we separated the two components of the disorder, generating two crystal structures (Figure 12), one for each component of the disorder (A and B). The structural comparison of A and B with the ten predictions for 3-Me, produced a match with predictions 3-Me05 and 3-Me06. Interestingly,

these two predictions corresponded to the those with the smoothest normalized structural rugosity ($\bar{R}^N_{depth}$) (see Figure 6).

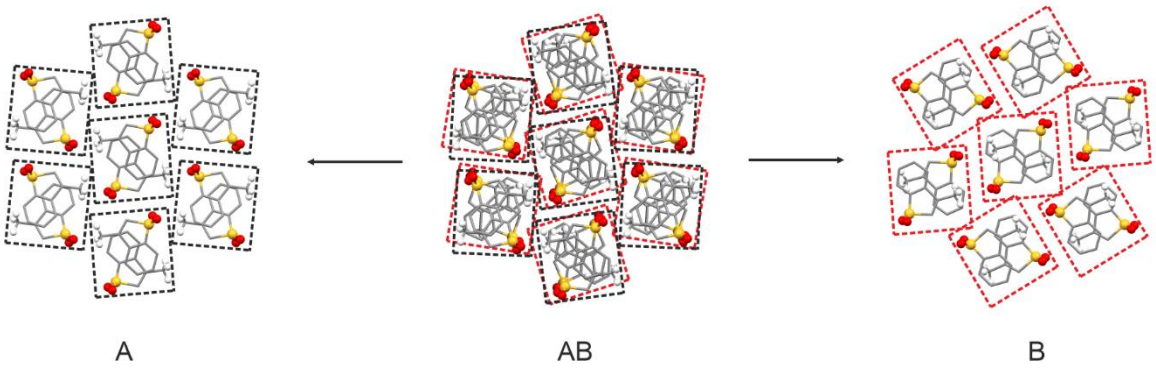

Figure 12. Crystal packing of the two components of the disorder A and B

In the case of 23-Me, the comparison of 23- Me β with the ten predictions only resulted in 1-D and 2-D similarities. We decided then to search for this new polymorph among the initial list of non-optimized structures generated by Asmadi and co-workers.[36] The results of the comparison shows that 23-Me β corresponds to rank 96, which was in the original paper not selected for optimization in view of the very high energy. After optimization, this prediction dropped to rank number 16. The normalized structural rugosity of the new polymorph was then calculated and compared with those obtained for the ten predictions for the 23-Me compound (Figure 13).

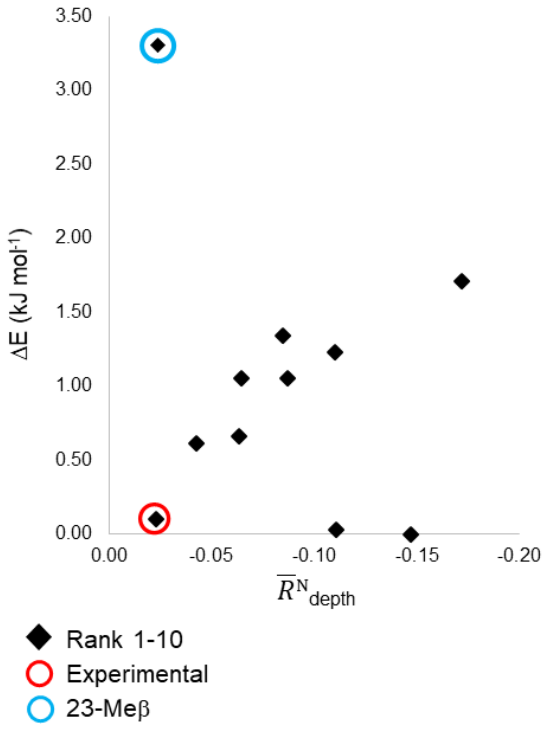

Figure 13. Relative lattice energy (ΔE) versus normalized average crystal rugosity ($\bar{R}^{N}_{depth}$) for 23-Me. The experimental structures 23-Me (CSD code GAPMAL) and the new polymorph 23-Meβ are circled in red and light-blue.

Conclusions.

In this study, we have analyzed the energy landscapes of three substituted methyl derivatives of the target compound benzo[b]thiophene 1,1-dioxide, by using crystal structure comparisons and the structural rugosity model. Our results suggest that this approach might be very useful to identify which putative structure might be amenable to experimental discovery.

The results of the crystal structure comparisons of the ten lowest energy predictions provided useful information on the presence of some robust molecular arrangements, particularly 1-D and 2-D motifs. We observed that in the majority of the structures, molecules are stacked to form two types of 1-D arrangements, named as S1 and S2. This was not the case of the 2-Me derivative, in which these two arrangements have been observed only in few predictions, including the one corresponding to the known experimental structure (2-Me01).

The analysis also allowed us observe that, for some pair of predictions, the transformation from one type of crystal packing to the other, would only require simple relative shifts of adjacent 2-D arrangements. Considering the small differences in the calculated lattice energies, we cannot exclude that these polymorphs, in a hypothetical crystallization experiment, would convert one into the other at nucleation/crystal growth stage or by proper solid-solid phase transitions. This raised the question whether only few of these predictions can effectively be experimentally isolated.

The application of the normalized structural rugosity, a parameter that, as described earlier, correlates structural surface rugosity and ease of crystallization, produced further insights on the search for new polymorphs. The results show that, for each ELS, the ten predictions lye within 0.2 units of rugosity from the smoothest polymorph. In this respect, they would all represent isolatable polymorphs. However, it is interesting to note that in most of the cases, there seems to be a correlation between the smoothest prediction of each ELS and the possibility to effectively isolate the corresponding experimental structure. This is particularly evident in the case of 3-Me and 23-Me, where the newly discovered polymorphs 3-Me β and 23-Me β and the known polymorph 23-Me α are all among the smoothest predictions. Furthermore, in the case of the 2-Me derivative, the only known experimental structure represent the most stable prediction and, together with prediction 2-Me10 (isomorphous with the known experimental structure GAPMAL), among the smoothest.

The experimental screening, limited to few common solvents and crystallizations from the melt, produced the evidence of a polymorphic behavior only in the case of 3-methyl and the 23-dimethyl derivatives. Crystallizations from the melt proved to be a simple and selective way to experimentally isolate the two new polymorphs 3-Me β and 23-Me β, while crystallizations from solvents always produced the already known experimental structures. In particular, the new polymorph 3-Me β showed two-fold disorder. A crystal structure comparison of the structures generated selecting each of the two possible components of the disorder, with the ten lowest energy predictions for the 3-Me derivative showed a match with predictions 3-Me05 and 3-Me06.

In the case of the 23-Me derivative, the comparison of new polymorphs 23-Me β with the predictions did not produce any relevant similarity, however, a search of this new polymorph among the non-optimized structures generated by Asmadi and co-workers.[36] produced a match with rank 96. After optimization, this prediction dropped to rank number 16. Interestingly, when we calculated the structural rugosity parameter for this new polymorph it showed a smooth value, very similar to that measured for the known structure (GAPMAL[38]).

Although, as pointed out by Cruz-Cabeza and co-workers, this model is not infallible,[12] we believe it certainly represent a valuable approach, especially if combined with all the other tools available for polymorphism screening.

Associated Content

Supporting Information

The Supporting Information is available free of charge on the

ACS Publications website at DOI:

S1: Synthetic Procedures; S2: Experimental Characterization; S3: XPac Analysis; S4: Crystal Packing Differences.

Author Information

Corresponding Author

*E-mail: riccardo.montis@uniurb.it.

ORCID: https://orcid.org/ 0000-0001-5239-1849

Author Contributions

The manuscript was written through contributions of all authors. All authors have given approval to the final version of the manuscript

Notes

The authors dedicate this work to the memory of Professor Frank J. Leusen

Acknowledgements

RM would like to thank Dr Nikolay Tumanov and Dr. Peter N. Horton for assistance with Crystallographic Information Files and Dr. Aurora Cruz-Cabeza for providing a copy of the Python script to calculate the normalized structural rugosity.

References

(1) Price, S. L. Why Don't We Find More Polymorphs? *Acta Crystallogr. Sect. B* **2013**, *69* (4), 313–328. https://doi.org/10.1107/S2052519213018861.

(2) Cruz-Cabeza, A. J.; Reutzel-Edens, S. M.; Bernstein, J. Facts and Fictions about Polymorphism. *Chem. Soc. Rev.* **2015**, *44* (23), 8619–8635. https://doi.org/10.1039/C5CS00227C.

(3) Cruz-Cabeza, A. J.; Feeder, N.; Davey, R. J. Open Questions in Organic Crystal Polymorphism. *Commun. Chem.* **2020**, *3* (1), 142. https://doi.org/10.1038/s42004-020-00388-9.

(4) McCrone, W. C. *Physics and Chemistry of the Organic Solid State*; Fox, D., Labes, M. M. & Weissberger, A., Ed.; Wiley, New York, 1965.

(5) Threlfall, T. L. Analysis of Organic Polymorphs. A Review. *Analyst* **1995**, *120* (10), 2435–2460. https://doi.org/10.1039/AN9952002435.

(6) Bernstein, J. *Polymorphism in Molecular Crystals*; Oxford University Press, 2010; Vol. 9780199236. https://doi.org/10.1093/acprof:oso/9780199236565.001.0001.

(7) Chemburkar, S. R.; Bauer, J.; Deming, K.; Spiwek, H.; Patel, K.; Morris, J.; Henry, R.; Spanton, S.; Dziki, W.; Porter, W.; Quick, J.; Bauer, P.; Donaubauer, J.; Narayanan, B. A.; Soldani, M.; Riley, D.; McFarland, K. Dealing with the Impact of Ritonavir Polymorphs on the Late Stages of Bulk Drug Process Development. *Org. Process Res. Dev.* **2000**, *4* (5), 413–417. https://doi.org/10.1021/op000023y.

(8) Rietveld, I. B.; Céolin, R. Rotigotine: Unexpected Polymorphism with Predictable Overall Monotropic Behavior. *J. Pharm. Sci.* **2015**, *104* (12), 4117–4122. https://doi.org/10.1002/jps.24626.

(9) Price, S. L.; Reutzel-Edens, S. M. The Potential of Computed Crystal Energy

Landscapes to Aid Solid-Form Development. *Drug Discov. Today* **2016**, *21* (6), 912–923. https://doi.org/https://doi.org/10.1016/j.drudis.2016.01.014.

(10) Kalash, L. N.; Cole, J. C.; Copley, R. C. B.; Edge, C. M.; Moldovan, A. A.; Sadiq, G.; Doherty, C. L. First Global Analysis of the GSK Database of Small Molecule Crystal Structures. *CrystEngComm* **2021**. https://doi.org/10.1039/D1CE00665G.

(11) Sacchi, P.; Reutzel-Edens, S. M.; Cruz-Cabeza, A. J. The Unexpected Discovery of the Ninth Polymorph of Tolfenamic Acid. *CrystEngComm* **2021**, *23* (20), 3636–3647. https://doi.org/10.1039/D1CE00343G.

(12) Montis, R.; Davey, R. J.; Wright, S. E.; Woollam, G. R.; Cruz-Cabeza, A. J. Transforming Computed Energy Landscapes into Experimental Realities: The Role of Structural Rugosity. *Angew. Chemie Int. Ed. n/a* (n/a). https://doi.org/10.1002/anie.202006939.

(13) Price, S. L.; Braun, D. E.; Reutzel-Edens, S. M. Can Computed Crystal Energy Landscapes Help Understand Pharmaceutical Solids? *Chem. Commun.* **2016**, *52* (44), 7065–7077. https://doi.org/10.1039/C6CC00721J.

(14) Shtukenberg, A. G.; Hu, C. T.; Zhu, Q.; Schmidt, M. U.; Xu, W.; Tan, M.; Kahr, B. The Third Ambient Aspirin Polymorph. *Cryst. Growth Des.* **2017**, *17* (6), 3562–3566. https://doi.org/10.1021/acs.cgd.7b00673.

(15) Neumann, M. A.; van de Streek, J.; Fabbiani, F. P. A.; Hidber, P.; Grassmann, O. Combined Crystal Structure Prediction and High-Pressure Crystallization in Rational Pharmaceutical Polymorph Screening. *Nat. Commun.* **2015**, *6* (1), 7793. https://doi.org/10.1038/ncomms8793.

(16) Bond, A. D.; Solanko, K. A.; Parsons, S.; Redder, S.; Boese, R. Single Crystals of Aspirin Form II: Crystallisation and Stability. *CrystEngComm* **2011**, *13* (2), 399–401. https://doi.org/10.1039/C0CE00588F.

(17) Kras, W.; Carletta, A.; Montis, R.; Sullivan, R. A.; Cruz-Cabeza, A. J. Switching Polymorph Stabilities with Impurities Provides a Thermodynamic Route to Benzamide Form III. *Commun. Chem.* **2021**, *4* (1), 38. https://doi.org/10.1038/s42004-021-00473-7.

(18) Liu, Y.; Gabriele, B.; Davey, R. J.; Cruz-Cabeza, A. J. Concerning Elusive Crystal Forms: The Case of Paracetamol. *J. Am. Chem. Soc.* **2020**, *142* (14), 6682–6689. https://doi.org/10.1021/jacs.0c00321.

(19) Neumann, M. A.; Leusen, F. J. J.; Kendrick, J. A Major Advance in Crystal Structure Prediction. *Angew. Chemie Int. Ed.* **2008**, *47* (13), 2427–2430.

https://doi.org/https://doi.org/10.1002/anie.200704247.

(20) Bowskill, D. H.; Sugden, I. J.; Konstantinopoulos, S.; Adjiman, C. S.; Pantelides, C. C. Crystal Structure Prediction Methods for Organic Molecules: State of the Art. *Annu. Rev. Chem. Biomol. Eng.* **2021**, *12* (1), 593–623. https://doi.org/10.1146/annurev-chembioeng-060718-030256.

(21) Montis, R.; Hursthouse, M. B.; Chan, H. C. S.; Kendrick, J.; Leusen, F. J. J. Experimental and Theoretical Investigations of the Polymorphism of 5-Chloroacetoxybenzoic Acid (5-Chloroaspirin). *CrystEngComm* **2012**, *14* (5), 1672–1680. https://doi.org/10.1039/C2CE06313A.

(22) Kendrick, J.; Montis, R.; Hursthouse, M. B.; Leusen, F. J. J. "In-Silico Seeding": Isostructurality and Pseudoisostructurality in a Family of Aspirin Derivatives. *Cryst. Growth Des.* **2013**, *13* (7), 2906–2915. https://doi.org/10.1021/cg4003324.

(23) Braun, D. E.; Gelbrich, T.; Jetti, R. K. R.; Kahlenberg, V.; Price, S. L.; Griesser, U. J. Colored Polymorphs: Thermochemical and Structural Features of N-Picryl- p-Toluidine Polymorphs and Solvates. *Cryst. Growth Des.* **2008**, *8* (6), 1977–1989. https://doi.org/10.1021/cg8000224.

(24) Braun, D. E.; Ardid-Candel, M.; D'Oria, E.; Karamertzanis, P. G.; Arlin, J.-B.; Florence, A. J.; Jones, A. G.; Price, S. L. Racemic Naproxen: A Multidisciplinary Structural and Thermodynamic Comparison with the Enantiopure Form. *Cryst. Growth Des.* **2011**, *11* (12), 5659–5669. https://doi.org/10.1021/cg201203u.

(25) Sacchi, P.; Lusi, M.; Cruz-Cabeza, A. J.; Nauha, E.; Bernstein, J. Same or Different – That Is the Question: Identification of Crystal Forms from Crystal Structure Data. *CrystEngComm* **2020**, *22* (43), 7170–7185. https://doi.org/10.1039/D0CE00724B.

(26) Hursthouse, M. B.; Montis, R.; Tizzard, G. J. Intriguing Relationships and Associations in the Crystal Structures of a Family of Substituted Aspirin Molecules. *CrystEngComm* **2010**, *12* (3), 953–959. https://doi.org/10.1039/b919538f.

(27) Hursthouse, M. B.; Montis, R.; Tizzard, G. J. Further Crystal Structures for the Substituted Aspirin Family of Molecules: The First Aspirin Carboxylate Catemer and a Detailed Assessment of the Subtle Influences of Weak Intermolecular Interactions. *CrystEngComm* **2011**, *13* (10), 3390–3401. https://doi.org/10.1039/C0CE00838A.

(28) Montis, R.; Hursthouse, M. B. Crystalline Adducts of Some Substituted Salicylic Acids with 4-Aminopyridine{,} Including Hydrates and Solvates: Contact and Separated Ionic Complexes with Diverse Supramolecular Synthons. *CrystEngComm* **2012**, *14* (21), 7466–7478. https://doi.org/10.1039/C2CE26008E.

(29) Montis, R.; Hursthouse, M. B. Surprisingly Complex Supramolecular Behaviour in the Crystal Structures of a Family of Mono-Substituted Salicylic Acids. *CrystEngComm* **2012**, *14* (16), 5242–5254. https://doi.org/10.1039/C2CE25336D.

(30) Hacıvelioğlu, F.; Montis, R.; Davies, D. B.; Kılıç, A.; Hursthouse, M. B.; Coles, S. J. Enantiotropic Conformational Polymorphism in 2{,}2{,}4{,}4-Bis-(2′{,}2′-Dimethylpropane-1′{,}3′-Dioxy)-6{,}6-Dichlorocyclotriphosphazene. *CrystEngComm* **2011**, *13* (12), 4102–4109. https://doi.org/10.1039/C1CE05163F.

(31) Gelbrich, T.; Hursthouse, M. B. A Versatile Procedure for the Identification{,} Description and Quantification of Structural Similarity in Molecular Crystals. *CrystEngComm* **2005**, *7* (53), 324–336. https://doi.org/10.1039/B502484F.

(32) Childs, S. L.; Wood, P. A.; Rodríguez-Hornedo, N.; Reddy, L. S.; Hardcastle, K. I. Analysis of 50 Crystal Structures Containing Carbamazepine Using the Materials Module of Mercury CSD. *Cryst. Growth Des.* **2009**, *9* (4), 1869–1888. https://doi.org/10.1021/cg801056c.

(33) Bryant, M. J.; Maloney, A. G. P.; Sykes, R. A. Predicting Mechanical Properties of Crystalline Materials through Topological Analysis. *CrystEngComm* **2018**, *20* (19), 2698–2704. https://doi.org/10.1039/C8CE00454D.

(34) Belenguer, A. M.; Cruz-Cabeza, A. J.; Lampronti, G. I.; Sanders, J. K. M. On the Prevalence of Smooth Polymorphs at the Nanoscale: Implications for Pharmaceuticals. *CrystEngComm* **2019**, *21* (13), 2203–2211. https://doi.org/10.1039/C8CE02098A.

(35) Liu, Y.; Black, J. F. B.; Boon, K. F.; Cruz-Cabeza, A. J.; Davey, R. J.; Dowling, R. J.; George, N.; Hutchinson, A.; Montis, R. When Crystals Do Not Grow: The Growth Dead Zone. *Cryst. Growth Des.* **2019**, *19* (8), 4579–4587. https://doi.org/10.1021/acs.cgd.9b00478.

(36) Asmadi, A.; Kendrick, J.; Leusen, F. J. J. Crystal Structure Prediction and Isostructurality of Three Small Molecules. *Chem. – A Eur. J.* **2010**, *16* (42), 12701–12709. https://doi.org/https://doi.org/10.1002/chem.200903227.

(37) El Amoudi El Faghi, M. S.; Geneste, P.; Olivé, J. L.; Rambaud, J.; Declercq, J.-P. Comparison of X-Ray Structure of 2- and 3-Methylbenzo[{\it B}]Thiophene 1,1-Dioxides. *Acta Crystallogr. Sect. C* **1988**, *44* (3), 498–500. https://doi.org/10.1107/S0108270187010680.

(38) El Amoudi El Faghi, M. S.; Geneste, P.; Olivé, J. L.; Dubourg, A.; Rambaud, J.; Declercq, J.-P. Structures of Benzo[b]Thiophene 1,1-Dioxide (a Redetermination) and of 2,3-Dimethylbenzo[b]Thiophene 1,1-Dioxide and 2-Bromobenzo[b]Thiophene 1,1-

Dioxide. *Acta Crystallogr. Sect. C* **1987**, *43* (12), 2421–2424. https://doi.org/https://doi.org/10.1107/S0108270187087559.

(39) Kawai, S.; Nakashima, T.; Kutsunugi, Y.; Nakagawa, H.; Nakano, H.; Kawai, T. Photochromic Amorphous Molecular Materials Based on Dibenzothienylthiazole Structure. *J. Mater. Chem.* **2009**, *19* (22), 3606–3611. https://doi.org/10.1039/B823354C.

(40) Fournier Dit Chabert, J.; Joucla, L.; David, E.; Lemaire, M. An Efficient Phosphine-Free Palladium Coupling for the Synthesis of New 2-Arylbenzo[b]Thiophenes. *Tetrahedron* **2004**, *60* (14), 3221–3230. https://doi.org/https://doi.org/10.1016/j.tet.2004.02.011.

(41) Buchwald, S. L.; Fang, Q. An Efficient One-Pot Method for the Preparation of Polysubstituted Benzothiophenes. *J. Org. Chem.* **1989**, *54* (12), 2793–2797. https://doi.org/10.1021/jo00273a006.

(42) Hooft, R. W. W. COLLECT. Nonius BV, Delft, The Netherlands. 1998.

(43) Otwinowski, Z. & Minor, W. Methods in Enzymology; C. W. Carter Jr & R. M. Sweet, Ed.; New York, USA, 1997; pp 307–326.

(44) Sheldrick, G. M. {\it SHELXT} {--} Integrated Space-Group and Crystal-Structure Determination. *Acta Crystallogr. Sect. A* **2015**, *71* (1), 3–8. https://doi.org/10.1107/S2053273314026370.

(45) Sheldrick, G. M. Crystal Structure Refinement with {\it SHELXL}. *Acta Crystallogr. Sect. C* **2015**, *71* (1), 3–8. https://doi.org/10.1107/S2053229614024218.

(46) Dolomanov, O. V; Bourhis, L. J.; Gildea, R. J.; Howard, J. A. K.; Puschmann, H. {\it OLEX2}: A Complete Structure Solution, Refinement and Analysis Program. *J. Appl. Crystallogr.* **2009**, *42* (2), 339–341. https://doi.org/10.1107/S0021889808042726.

(47) Sheldrick, G. M. SADABS. University of Göttingen, Germany 1996.

(48) Fabbiani, F. P. A.; Dittrich, B.; Florence, A. J.; Gelbrich, T.; Hursthouse, M. B.; Kuhs, W. F.; Shankland, N.; Sowa, H. Crystal Structures with a Challenge: High-Pressure Crystallisation of Ciprofloxacin Sodium Salts and Their Recovery to Ambient Pressure. *CrystEngComm* **2009**, *11* (7), 1396–1406. https://doi.org/10.1039/B822987B.

(49) Burger, A.; Koller, K. T. Polymorphism and Pseudopolymorphism on Nifedipine. *Sci. Pharm.* **1996**, *64* (3–4), 293–301.

(50) Su, Y.; Xu, J.; Shi, Q.; Yu, L.; Cai, T. Polymorphism of Griseofulvin: Concomitant Crystallization from the Melt and a Single Crystal Structure of a Metastable

Polymorph with Anomalously Large Thermal Expansion. *Chem. Commun.* **2018**, *54* (4), 358–361. https://doi.org/10.1039/C7CC07744K.

For Table of Contents Use Only

Combining structural rugosity and crystal packing comparison: A route to more polymorphs?

Riccardo Montis[a,b]*, Michael B Hursthouse[b], John Kendrick[c], Jason Howe[b] and Richard J. Whitby[b].

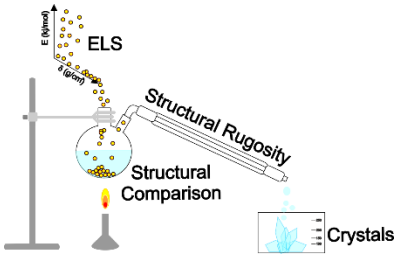

In this study structural comparisons and the rugosity model are combined to investigate experimental and predicted crystal structures of three rigid and planar small molecules: 2-methyl-, 3-methyl- and 2,3-dimethyl-benzo[b]thiophene 1,1-dioxide. The results suggest that this approach might help in rationalizing which predicted crystal structure may be accessible by experiments.